ACES Asian Chemical Editorial Society

doi.org/10.1002/asia.202300773

CHEMISTRY AN ASIAN JOURNAL Research Article

www.chemasianj.org

Special Collection

Unravelling the Effect of Acid-Driven Electron Transfer in High-Valent $Fe^{IV}=O/Mn^{IV}=O$ Species and Its Implications for Reactivity

Neethinathan Johnee Britto,[a] Asmita Sen,[a] and Gopalan Rajaraman*[a]

The electron transfer (ET) step is one of the crucial processes in biochemical redox reactions that occur in nature and has been established as a key step in dictating the reactivity of high-valent metal-oxo species. Although metalloenzymes possessing metal-oxo units at their active site are typically associated with outer-sphere electron transfer (OSET) processes, biomimetic models, in contrast, have been found to manifest either an inner-sphere electron transfer (ISET) or OSET mechanism. This distinction is clearly illustrated through the behaviour of $[(N4Py)Mn^{IV}(O)]^{2+}$ (**1**) and $[(N4Py)Fe^{IV}(O)]^{2+}$ (**2**) complexes, where complex **1** showcases an OSET mechanism, while complex **2** exhibits an ISET mechanism, especially evident in their reactions involving C–H bond activation and oxygen atom transfer reactions in the presence of a Lewis/Bronsted acid. However, the precise reason for this puzzling difference remains elusive. This work unveils the origin of the perplexing inner-sphere vs outer-sphere electron transfer process (ISET vs OSET) in $[(N4Py)Mn^{IV}(O)]^{2+}$ (**1**) and $[(N4Py)Fe^{IV}(O)]^{2+}$ (**2**) species in the presence of Bronsted acid. The calculations indicate that when the substrate (toluene) approaches both **1** and **2** that is hydrogen bonded with two HOTf molecules (denoted as **1-HOTf** and **2-HOTf**, respectively), proton transfer from one of the HOTf molecules to the metal-oxo unit is triggered and a simultaneous electron transfer occurs from toluene to the metal centre. Interestingly, the preference for OSET by **1-HOTf** is found to originate from the choice of $Mn^{IV}=O$ centre to abstract spin-down (β) electron from toluene to its $\delta(d_{xy})$ orbital. On the other hand, in **2-HOTf**, a spin state inversion from triplet to quintet state takes place during the proton (from HOTf) coupled electron transfer (from toluene) preferring a spin-up (α) electron abstraction to its $\sigma^*(d_z^2)$ orbital mediated by HOTf giving rise to ISET. In addition, **2-HOTf** was calculated to possess a larger reorganisation energy, which facilitates the ISET process via the acid. The absence of spin-inversion and smaller reorganisation energy switch the mechanism to OSET for **1-HOTf**. Therefore, for the first time, the significance of spin-state and spin-inversion in the electron transfer process has been identified and demonstrated within the realm of high-valent metal-oxo chemistry. This discovery holds implications for the potential involvement of high-valent Mn-oxo species in performing similar transformative processes within Photosystem II.

Introduction

High-valent heme and nonheme metal oxo species act as key intermediates in various biological redox reactions.[1] In particular, the $Mn^{IV}=O$ species in the water oxidation reaction in the oxygen-evolving complex (OEC) in photosystem II[2] and $Fe^{IV}=O$ species in the C–H bond activation in cytochrome P450,[3] cytC3 enzymes[4] are notable. Inspired by these naturally occurring systems, various groups have made efforts to design biomimetic models of these enzymes. It has been noted that the reactivity of these biomimetic models is largely influenced by the nature and spin-states of the central metal ion, ligand architecture, and external additives such as the introduction of Lewis/Bronsted acids and redox inactive metal ions.[5] The intriguing reactivity pattern of these enzymes is intrinsically correlated to the mechanism of the electron transfer process, which is the fundamental step and the driving force for the observed reactivity.[6] While metalloenzymes containing metal-oxo units are generally known to react via the outer-sphere electron transfer process, the biomimetic models, on the other hand, exhibit either an inner-sphere electron transfer (ISET) or outer-sphere electron transfer (OSET) mechanisms. It is intriguing to note here that the soluble methane monooxygenase (sMMO) enzyme,[7] along with $[Fe^{IV}(O)(H_2O)_5]^{2+}$ species,[8] both of which are landmark examples of reactivity in this area, exhibit outer-sphere ET/PCET reactions. At the biomimetic front N4Py based $Mn^{IV}=O$ $[(N4Py)Mn^{IV}(O)]^{2+}$ (**1**) and $Fe^{IV}=O$ $[(N4Py)Fe^{IV}(O)]^{2+}$ (**2**) complexes towards strong C–H bonds in toluene have been studied in detail, and this study suggests that **1** follow OSET mechanism while **2** follow ISET mechanisms in the presence of triflic acid and scandium triflate.[9] A careful look at the literature report reveals that $Mn^{IV}=O$ in the presence of Lewis/Bronsted acids react via OSET, while $Fe^{IV}=O$ exhibit either ISET or OSET (Table 1). While extensive experimental studies have been reported, theoretical studies to understand the origin of the preference in the mechanism are not established. As this is a fundamental step that controls the reactivity of the catalyst

[a] Dr. N. J. Britto, Dr. A. Sen, Dr. G. Rajaraman
Department of Chemistry, Indian Institute of Technology Bombay, Powai, Mumbai 400 076, (India)
E-mail: rajaraman@chem.iitb.ac.in

Supporting information for this article is available on the WWW under https://doi.org/10.1002/asia.202300773

Special Collection This manuscript is part of a special collection on 3rd International Conference on Organometallics and Catalysis (ICOC-2023).

Table 1. Some representative ET mechanism reported for different reactions by various representative metal-oxo species.

Complex /oxidant	Lewis/ Bronsted Acid	Substrate /Reductant	ET Mechanism	λ	Ref.
di(μ-oxo)diiron(IV) unit of sMMO enzyme	-	CH_4	PC-OSET	–	[7]
$[Fe^{IV}(H_2O)_5O]^{2+}$	$HClO_4$	$Fe(Cp)(C_5H_4CH_2OH)$, $IrCl_6^{3-}$, $Os(phen)_3^{2+}$	OSET	–	[8]
$[Fe^{IV}(H_2O)_5O]^{2+}$	$HClO_4$	$Ni(cyclam)^{2+}$, Ce(III)	ISET	–	[8]
$[(TMC)Fe^{IV}(O)]^{2+}$ $[(Bn\text{-}TPEN)\ Fe^{IV}(O)]^{2+}$, $[(N4Py)Fe^{IV}(O)]^{2+}$	–	ferrocene derivatives	–	2.37 2.55 2.74	[15]
[(N4Py) $Mn^{IV}(O)]^{2+}$ and $[(Bn\text{-}TPEN)Mn^{IV}(O)]^{2+}$	HOTf	1,4-cyclohexadiene para-X-substituted-thioanisoles	OSET	2.20	[13]
$[(N4Py)Fe^{IV}(O)]^{2+}$	$HClO_4$	thioanisoles	ISET	2.74	[15]
$[(dpaq^{5H,Cl})Mn^{III}(OH_2)]^{2+}$	HOTf	4-methoxy-2,6-di-tert-butylphenol	OSET	–	[33]
[(dpaq)- $Mn^{III}(OH_2)]^{2+}$	–	thioanisole and triphenylphosphine derivatives	OSET	2.09	[34]
$[(N4Py)Mn^{IV}(O)]^{2+}$-$(HOTf)_2$	HOTf	styrene, thioanisole, and toluene	OSET	2.23	[35]

towards hydrogen atom transfer (HAT) and oxygen atom transfer (OAT) reactions, deciphering the origin of electron transfer is key to the design of future catalysts.[10] In this work, employing DFT and ab initio CASSCF calculations, we have examined in detail the factors that dictate the mechanism of electron transfer considering complexes **1** and **2**.

Results and Discussion

Electronic Structure of 1, 2, 1-HOTf and 2-HOTf

Initially, DFT calculations [(UB3LYP-D3/def2-TZVPP//UB3LYP-D3/SDD(Fe),6-31G**(rest); PCM(MeCN)], see computational details) were performed on species **1** and **2** (Figure 1) to determine their respective ground states. The computed results predict a quartet $S = {}^3/_2$ spin state for species **1** and a triplet $S = 1$ spin state for **2** as the ground state which is in accordance with the earlier reports (Figure 2).[11,12] The spin density plots of all the species discussed are collected in Supporting Information, Figure S1–S4. The energy gap between the ground state and the first-excited spin state in the ladder for both **1** and **2** are nearly the same (39.9 kJ/mol vs 41.2 kJ/mol). Both X-ray and spectroscopic studies reveal that in the presence of triflic acid, the metal-oxo moiety in **1** coordinate with two HOTf molecules to form $[(N4Py)Mn^{IV}(O)]^{2+}$-$(HOTf)_2$ (denoted as **1-HOTf**).[13] In the case of **2**, the experimental report suggests a binding of two HOTf molecules to the Fe-oxo unit, leading to the formation of $[(N4Py)Fe^{IV}(O)]^{2+}$-$(HOTf)_2$ (denoted as **2-HOTf**).[9] The binding of two triflic acid molecules to **1** and **2** is found to be exothermic by −111.5 kJ/mol and −87.3 kJ/mol, respectively and does not alter the nature of the ground spin state in both cases. Further, ab initio CASSCF(9,8) calculations (see computational details) were performed on **1-HOTf**, which also yielded $S = 3/2$ ground state and suggested the same electronic configurations as DFT methods with very little mixing (99%), affirming confidence in the methodology chosen.

From Figure 1, it is conspicuous that the two triflic acids form a relatively stronger hydrogen bonding interactions (1.595 Å and 1.671 Å) with the $Mn^{IV}=O$ unit in **1** than with $Fe^{IV}=O$ moiety in **2** (1.694 Å and 1.719 Å), which corroborates the experimental suggestion.[9] This is attributed to the large negative charge on the oxo centre of $Mn^{IV}=O$ species (−0.416) as compared to the $Fe^{IV}=O$ (−0.261), reflecting their expected basicity. This is also reflected in the NBO second-order perturbation theory analysis, where stronger donor-acceptor interactions are found for **1** compared to **2** (124.7 kJ/mol vs 39.1 kJ/mol, Figure S5) – all implying stronger binding of triflic acid to **1** vis-à-vis **2**. The orbital evolution diagram of **1, 2, 1-HOTf** and **2-HOTf** were plotted (see Figure S6–S12 for orbital evolution diagram of all species). The d-orbital energy ordering for both **1** and **2**, and their HOTf bound congeners (**1-HOTf** and **2-HOTf**) is the same ($d_{xy} < d_{yz\sim dxz} < d_{x^2-y^2} < d_{z^2}$). However, the $\triangle E$ ($d_{x^2-y^2}$–d_{yz}/d_{xz}) of **2** (5.0 eV) is found to be higher as compared to **1** (4.1 eV). In the presence of triflic acids, the splitting are slightly reduced by 0.2 eV in **2-HOTf** (4.8 eV) and slightly increased by 0.2 eV in **1-HOTf** (4.3 eV).

Mechanism of Electron Transfer

To comprehend the electron transfer process, the substrate is taken to the vicinity of the triflic acid-bound catalyst to form a reactant complex (**RC**, Figure 1). This step is exothermic by 46.6 kJ/mol and 37.8 kJ/mol from **1-HOTf** and **2-HOTf**, respectively (Figure 1). A close examination of reactant complex species reveals that the substrate is anchored to the catalyst via several non-covalent interactions in $\mathbf{RC_{Mn}}$ and $\mathbf{RC_{Fe}}$ (Figure S13). Very strong C–H•••π interactions (2.602 Å and 2.479 Å for Mn and Fe, respectively) are noted between the π-electron of toluene and the pyridine σ(CH) atoms and this hold the substrate in the vicinity of the catalyst. Furthermore, a number of C–H•••O and C–H•••F interactions ranging from 2.5 Å–3.0 Å between the HOTf

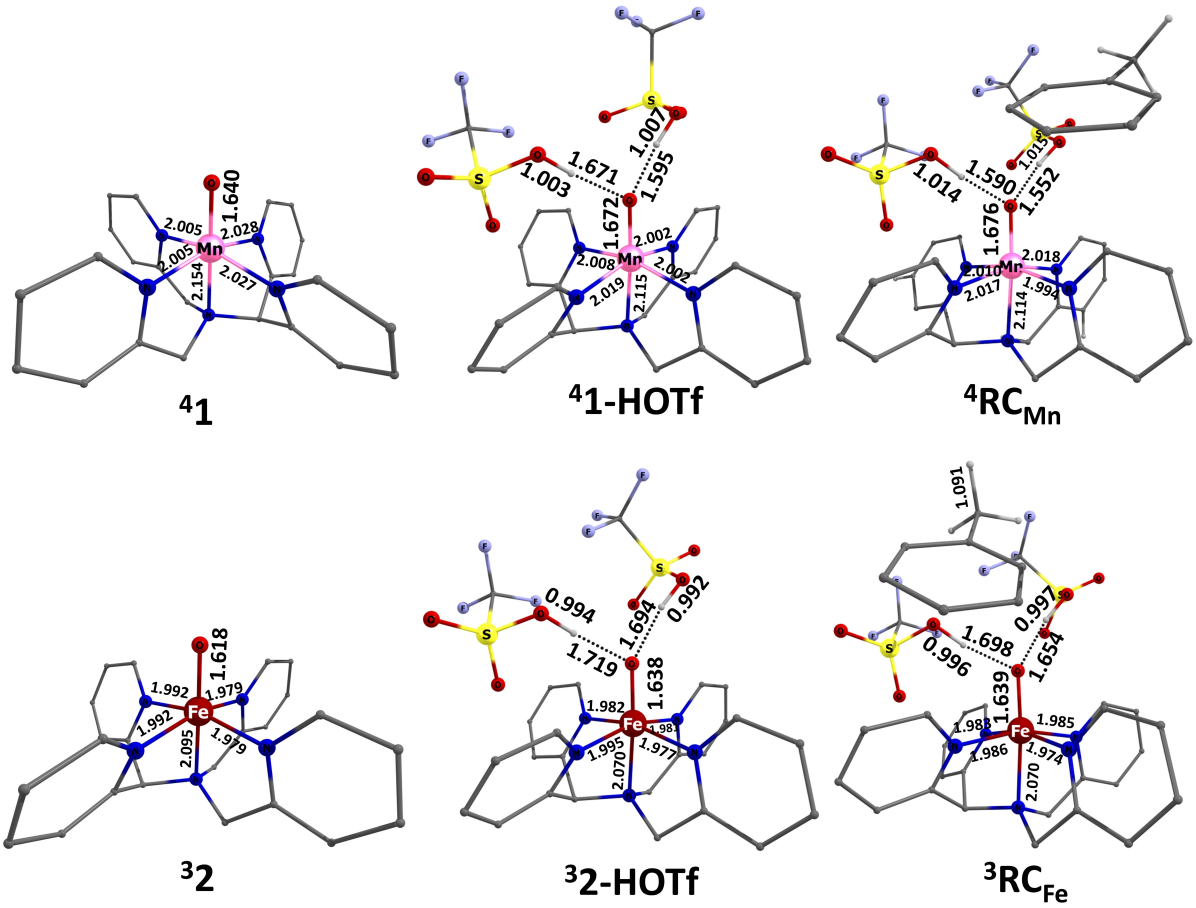

Figure 1. UB3LYP-D3 optimised ground state geometries of ^{4}**1**, ^{3}**2**, ^{4}**1-HOTf**, ^{3}**2-HOTf**, ^{4}**RC**$_{Mn}$ and ^{3}**RC**$_{Fe}$ with pertinent bond lengths in Å.

molecule and the substrate aid in stabilising the substrate. This indicates that the HOTf molecules attached to **1** and **2** help in stabilising the substrate before the electron transfer occurs. Attempts to optimize the substrate near the vicinity of the HOTf molecules prior to proton coupled electron transfer, resulted in the substrate reverting back to the orientation shown in Figure S13 for ^{4}**RC**$_{Mn}$ and ^{3}**RC**$_{Fe}$. A careful analysis reveals that no electron transfer, even partial has not taken place at this stage for both **1** and **2** (Figure S3 and Table S1). In the next step, the substrate moves to the vicinity of triflic acid generating another reactant complex (**RC**′). Figure 3 portrays the ground state optimized geometries and their respective spin density plots. At this stage when the substrate is at the vicinity of the acid, this triggers the proton-coupled electron transfer process where a proton is transferred from the triflic acid to the oxo oxygen atom and at the same time one electron is transferred from the substrate to the catalyst. Attempts to optimize the substrate near the ligand backbone after proton-coupled electron transfer process had taken place in **RC**′ resulted in the substrate orienting back to the vicinity of triflate anion as the substrate which is a cationic radical now prefers to be stabilized by interactions with the triflate anion. The formation of **RC**′ is slightly endothermic (22.9 kJ/mol) in the case of Mn, while this formation is thermoneutral for Fe. A careful MO/NBO analysis (Figure 1) reveals that at this stage, not only electron transfer from the substrate to the catalyst is triggered, but it also skews the spin-state energetics associated with a switch from S = 1 to high-spin S = 2 is observed for Fe. As the high-spin state is conventionally known as the reactive spin-state of Fe^{IV} = O species,[12,14] its stabilisation prior to the C–H bond activation transition state is intriguing. It suggests that the electron transfer step is pivotal to the reactivity, and this is independent of the nature of the substrates. This also rationalises the puzzling experimental observation that both HAT and OAT reactions could be unified as an electron transfer-driven process as, in both cases, it is the HOTf molecule that triggers the electron transfer process in the presence of the substrate, and the PCET occurs via proton donation from the HOTf with an electron found to be transferred from the substrate.[9a]

Electronic Origin of the OSET and ISET

In order to gain further insights into the ET mechanism, the orbital evolution diagram was analyzed in detail and a qualitative electron shift diagram is drawn in Figure 4. In the case of **RC**′ species, the electron transfer is triggered where a spin-down β-electron from the substrate is transferred to the δ(d_{xy}) orbital of Mn^{IV} = O unit, while in the case of Fe, a spin-up α -electron is transferred to the σ*(d_{z^2}) orbital. This is clearly seen in the spin

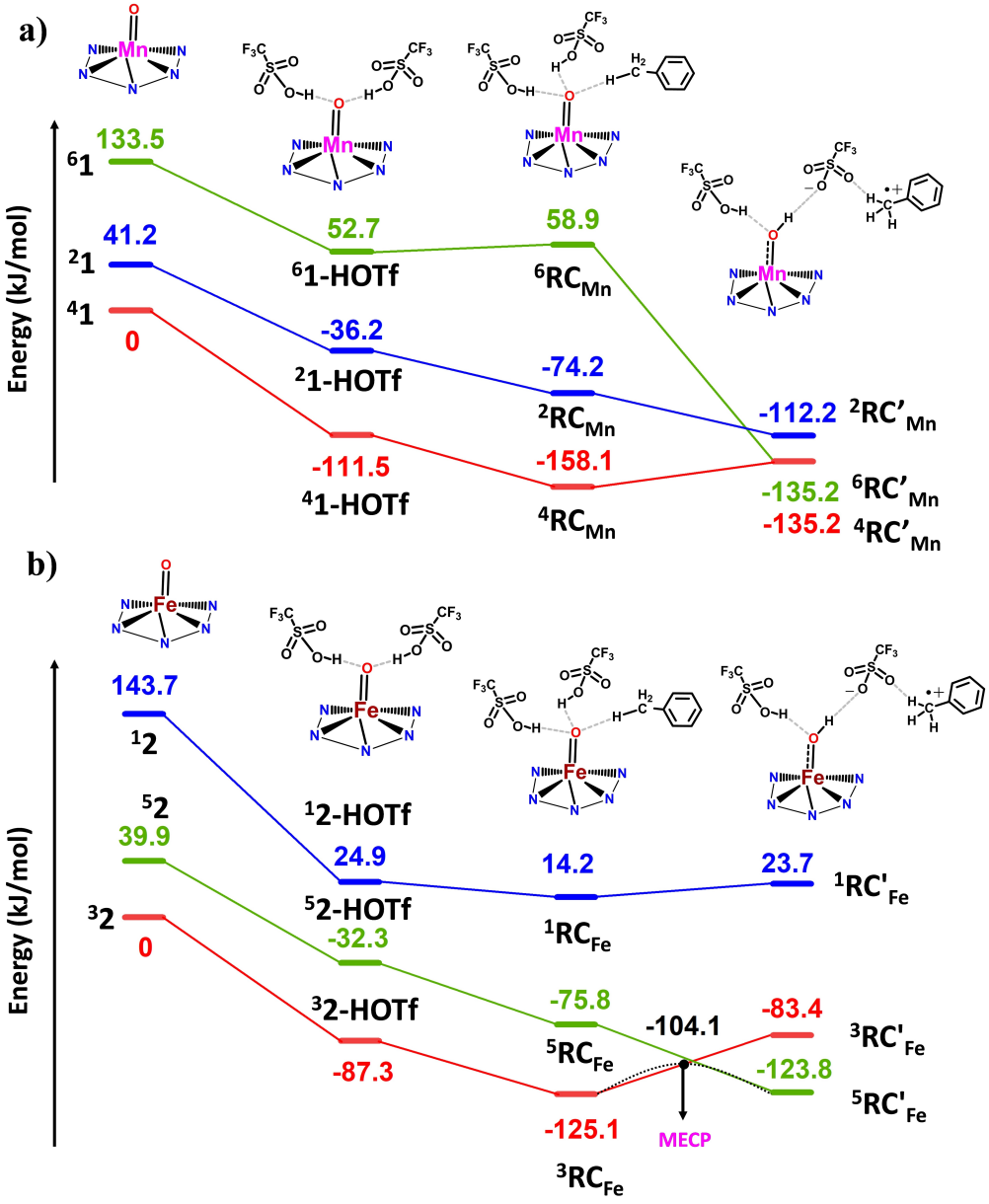

Figure 2. UB3LYP-D3 computed potential energy surface of (a) **1** and (b) **2** forming **1-HOTf** or **2-HOTf** followed by the anchoring of substrate to yield reactant complex **RC** and finally the proton coupled electron transfer in another reactant complex **RC′**.

density plots presented in Figure 3. A spin density of around −0.976 is localized on the substrate while on the Fe(IV) centre, the spin density is increased from 3.202 in ^{5}**RC**$_{Fe}$ to 4.227 in ^{5}**RC′**$_{Fe}$ indicating that an α-electron transfer had occurred at this stage. In the case of ^{4}**RC′**$_{Mn}$, a spin density of 0.894 is noted on the substrate while the spin density on Mn(IV) centre and oxo group is decreased from 2.677 and 0.413 in ^{4}**RC**$_{Mn}$ to 2.012 and 0.091 in ^{4}**RC′**$_{Mn}$ substantiating a β-electron transfer from substrate to the Mn^{IV}-oxo group. A careful look at the donor-acceptor MOs (Figure 5) in this electron transfer process reveals that in the case of Mn, the acceptor orbital is primarily metal-centric (d_{xy}) with a slight delocalisation to oxo and pyridinic ligands. The donor orbital is primarily substrate-centric (93%) with no contribution from triflic acid (0%) and a smaller contribution from the catalyst (7%), suggesting no direct involvement of triflic acid in the electron transfer process but rather via stronger CH$^{\bullet\bullet\bullet}\pi$ interactions of the ligand. The acceptor MO (β-HOMO of ^{4}**RC′**$_{Mn}$) is mainly catalyst centric (99%). This suggests an outer-sphere electron transfer process. This may be attributed to the choice of the orbital that the electron is being transferred. As the δ-type (d_{xy}) orbital with weak or little overlap with the oxo unit, the electron transfer via the ligand framework is the preferred choice, and hence it follows OSET processes. As Mn^{IV}=O species invariably exhibit S=3/2 ground state, the electron transfer to the d_{xy} is the preferred route (note the crystal field splitting of the d-orbital is larger for Mn), and this is consistent with the literature report that OSET is preferred for the Mn^{IV}=O species, in general (Table 1). Furthermore, this supports the experimental

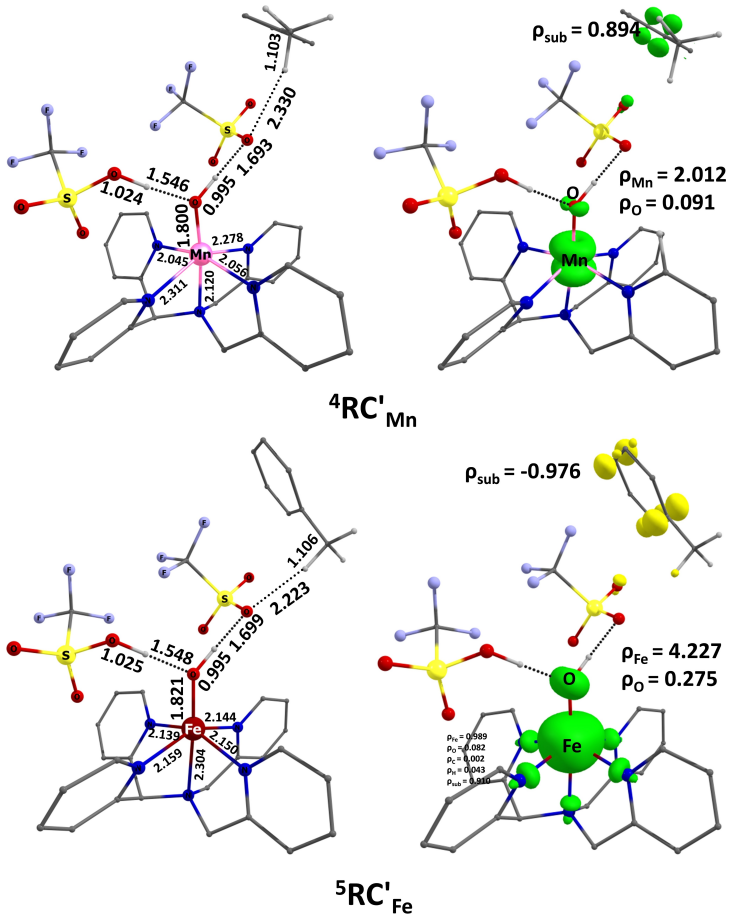

Figure 3. UB3LYP-D3 optimised ground state geometries and their corresponding spin density plots of $^{4}RC'_{Mn}$ and $^{5}RC'_{Fe}$.

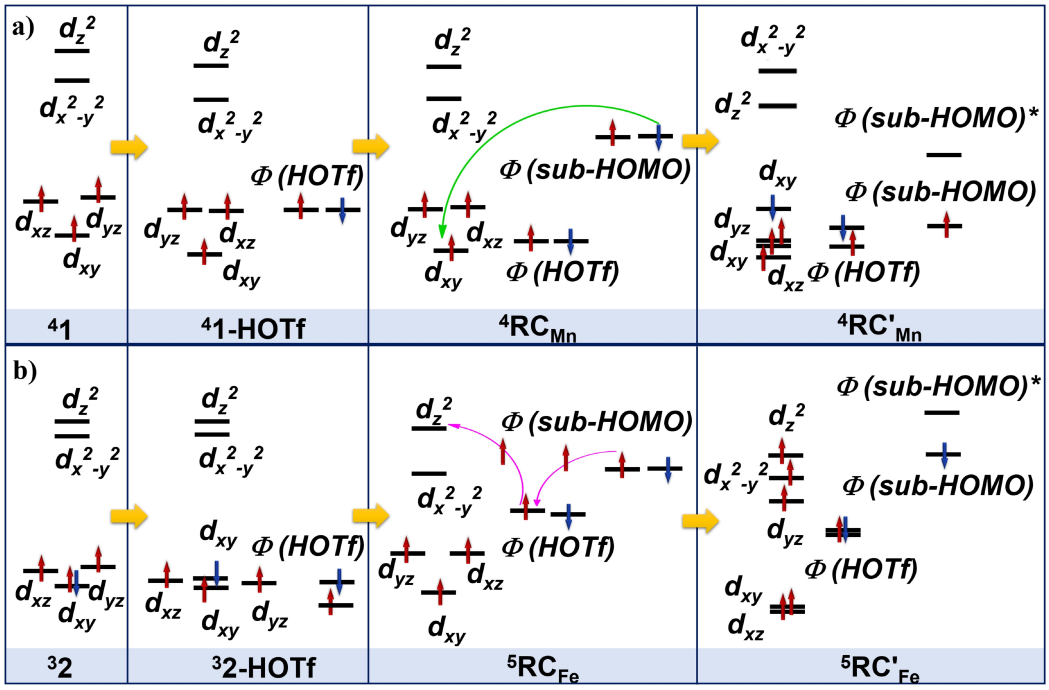

Figure 4. UB3LYP-D3 computed electron shift diagram showing the change in occupancies and electron transfer from (a) $^{4}1 \rightarrow {}^{4}1\text{-HOTf} \rightarrow {}^{4}RC_{Mn} \rightarrow {}^{4}RC'_{Mn}$ and (b) $^{3}2 \rightarrow {}^{3}2\text{-HOTf} \rightarrow {}^{5}RC_{Fe} \rightarrow {}^{5}RC'_{Fe}$. The orbital levels are only qualitative representation.

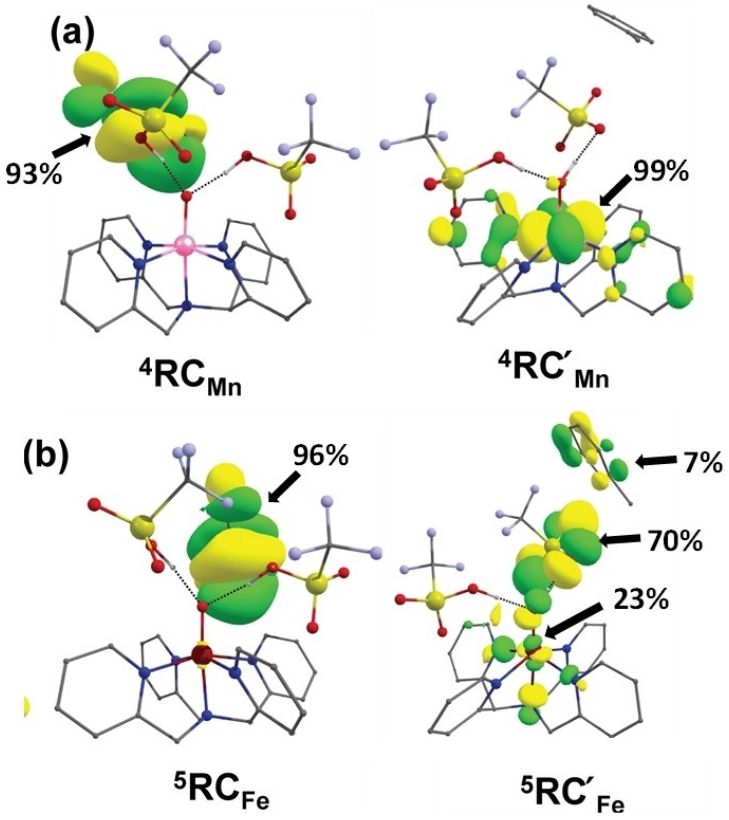

Figure 5. Computed donor→acceptor molecular orbitals of (a) $^4RC_{Mn}$-β-HOMO →$^4RC'_{Mn}$-β-HOMO and (b) 3RCFe-α-HOMO→$^5RC'_{Fe}$-α-HOMO.

observations that the reorganisation energy controls the reactivity, irrespective of the substrate.

In the case of $^5RC'_{Fe}$, an α- electron from the substrate was transferred to the σ*(d_z^2) orbital of the metal, and this electron transfer is routed via the triflic acid (Figure 5). The donor orbital ($^3RC_{Fe}$-α-HOMO) has significant substrate contribution (96%) with minor contributions from both acid and the catalyst (1% and 3%, respectively), while the acceptor orbital (after the electron transfer, i.e. α-HOMO $^5RC'_{Fe}$) has 70% contribution from one of the triflic acid with a substantial contribution from substrate π MOs and σ*(d_z^2) orbitals (7% and 23%, respectively). This suggests that the electron transfer from the π orbital of the substrate, which has strongly mixed with the triflic acid, is transferred to the triflic acid en route to the σ*(d_z^2) orbital of the metal (Figure 5). This discloses inner-sphere electron transfer mediated via the acid. This is also consistent with the experiments and earlier studies that indicate that Fe^{IV}=O with triplet ground state prefers ISET process.[8–9,15]

Interestingly, the electron transfer in the case of Fe^{IV}=O was found to begin from a triplet state and end with a quintet state suggesting a minimum energy crossing point (MECP)[16] that is mandatory to facilitate this electron transfer. We have computed the energetics cost of this MECP, and the corresponding transition state is located to be at 21.0 kJ/mol, suggesting an intrinsic barrier for the ET process. On the other hand, the Mn^{IV}=O species has no such kinetic hindrance. The analysis reveals that the electron transfer from the substrate to the catalyst is nearly completed at the MECP geometry, suggesting that both the spin-state crossover and ET processes coincide at the MECP. The electron transfer at the triplet state has a significant energy penalty for the following reasons (i) the σ*(d_z^2) orbital is strongly destabilised, and the HOTf orbital is strongly stabilised, leading to the donor-acceptor energy gap of 5.4 eV while in the same the gap in the quintet state is much smaller (3.9 eV). (ii) α-electron transfer in the triplet state lead to a $3k_{dd}$ unit of exchange stabilisation, while for the quintet state, it is found to be a $10k_{dd}$ unit, tilting the balance in favour of the quintet state ET process.[17a–b] Further modifying the ligand architecture, for example, by replacing one of the nitrogen atoms with an oxygen is expected to offer a weaker ligand environment leading to the stabilisation of S=2 spin state as the ground state for the Fe^{IV}=O species.[17c] This is expected to avoid the required MECP and therefore, can enhance the reactivity rate of electron transfer.

To further understand the electron-transfer process, we have performed a relaxed potential energy surface (PES) scan along the metal-oxo bond for various spin states of Fe^{IV}=O/Fe^{III}=O couple as well as Mn^{IV}=O/Mn^{III}=O couple in the presence of triflic acid (see Figure 6). One electron reduction of the Mn^{IV}=O leads to the stabilisation of Mn^{III}=O with a quintet ground state, and for the Fe^{III}=O species, the sextet state is found to be the ground state. From the developed PES, we have computed the reorganisation energy (λ_{DFT}).[18] The λ_{DFT} is found to be 2.42 eV and 2.90 eV for the Mn^{IV}=O/Mn^{III}=O and Fe^{IV}=O/Fe^{III}=O couples, respectively. This match excellently with the experimental λ values of 2.16 eV and 2.74 eV, respectively, offering confidence in the estimated parameters. From the computed

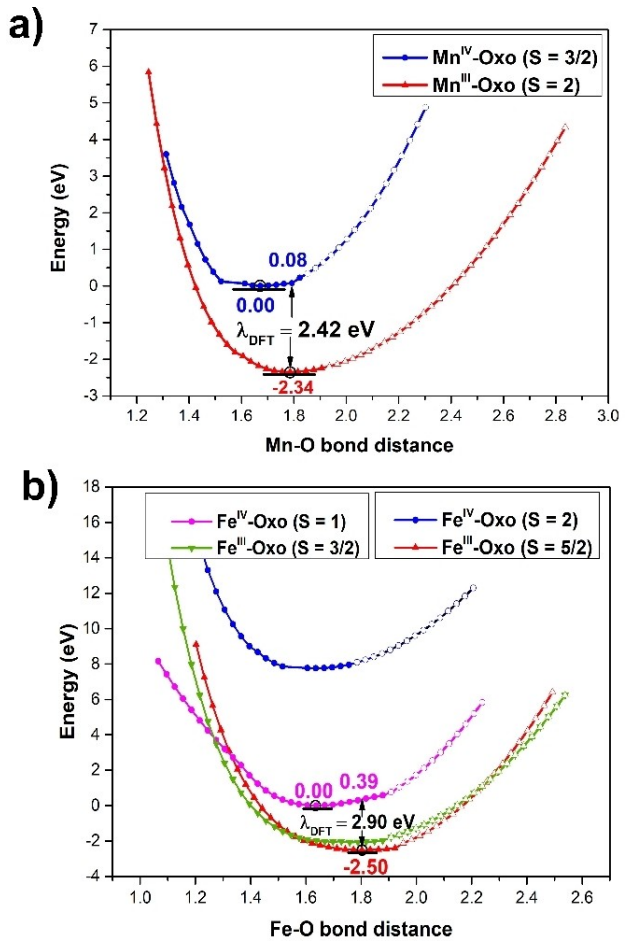

Figure 6. DFT computed reorganisation energy diagram for (a) $Mn^{IV}=O/Mn^{III}=O$ and (b) $Fe^{IV}=O/Fe^{III}=O$ couple.

λ_{DFT}, it is clear that for the $Mn^{IV}=O/Mn^{III}=O$ couple, the λ value is smaller. This is due to a flat MnIV=O surface upon elongation of the Mn…O bond from its equilibrium point to that of the $Mn^{III}=O$ distance. For the $Fe^{IV}=O/Fe^{III}=O$ couple, the surface is uphill leading to larger λ value (Figure 6 and S14 for inset). This difference is because of (i) the elongation of $Mn^{\bullet\bullet\bullet}O$ bond leads to the formation of MnIII–$O^{\bullet}$ species which is stabilised due to very strong H-bonding interactions from the two triflic acids, however for Fe^{III}–$O^{\bullet}$ species such strong H-bonding are missing. (ii) the additional electron enter into $\sigma^*(dz^2)$ orbital as the M–O bond elongates and this is stabilised significantly in case of Mn^{III}–$O^{\bullet}$ due to $Mn^{\uparrow\uparrow\uparrow\uparrow}$–$O^{\downarrow}$ configuration while in case of Fe^{III}–$O^{\bullet}$, $Fe^{\uparrow\downarrow\uparrow\downarrow\uparrow}$–$O^{\uparrow}$ configuration is found where α-electron on the oxo radical offer greater destabilisation of the $\sigma^*(d_z^2)$ orbital, demanding greater reorganisation energy. The spatial orientation or position of the catalyst with respect to the two HOTf molecules and the substrate are nearly same in both ^{4}**RC′**$_{Mn}$ and ^{5}**RC′**$_{Fe}$ species. This shows that the stereo-electronic factors cannot be the rationale for destabilizing the $\sigma^*(d_z^2)$ orbital and it is the transfer of α-electron on the oxo radical entity that contributes significantly to the observed higher reorganization energy. As the reorganisation energy for the $Fe^{IV}=O/Fe^{III}=O$ couple is larger, this prefers the ISET pathway, and for the $Mn^{IV}=O/Mn^{III}=O$ couple, the flat PES at the reactant lead to the OSET pathway. As the $Mn^{IV}=O/Mn^{III}=O$ couple follow the OSET pathway, we have performed a relaxed scan at the ^{4}**RC′**$_{Mn}$ geometry by varying the distance between the catalyst and substrate from 2.2 Å to 8.0 Å to perceive if the electron transfer is s short or long-range process. The scan performed (Figure S15) reveals that the electron transfer takes place between 3.5–4.0 Å window, suggesting that this is a relatively long-range OSET path. To affirm this, we have performed intrinsic bond orbital (IBO) calculations, which trace the mode of electron transfer, and these calculations suggest that one β-electron from the substrate is transferred to the $[(N4Py)Mn^{IV}(O)]^{2+}$-$(HOTf)_2$ unit even at a longer distance (see Figure 7). This affirms long-range outer-sphere electron transfer between the π MO of the substrate to the $\delta(d_{xy})$ orbital of the Mn ion. Further, as the reorganisation energy is correlated to the M–O bond lengths, attempts to vary this bond length via additional various flexible ligand systems are also expected to influence the reorganisation energy and rate of ET and hence the reactivity.[17d]

While the proposed mechanism is for Bronsted acid, we believe with Lewis acid such as $Sc(OTf)_3$, a similar mechanism without involvement of proton could be present. To obtain insights into this mechanism, we have performed additional calculations where dinuclear species of $Sc(OTf)_3$ coordinate to $Fe^{IV}=O/Mn^{IV}=O$ species (See Figure S16). The calculations reveal that the Mn–O distance is similar, while the Fe–O distance is significantly elongated at the triplet state, suggesting the development of Fe^{III}–$O^{\bullet}$ character upon binding with Sc-triflate.

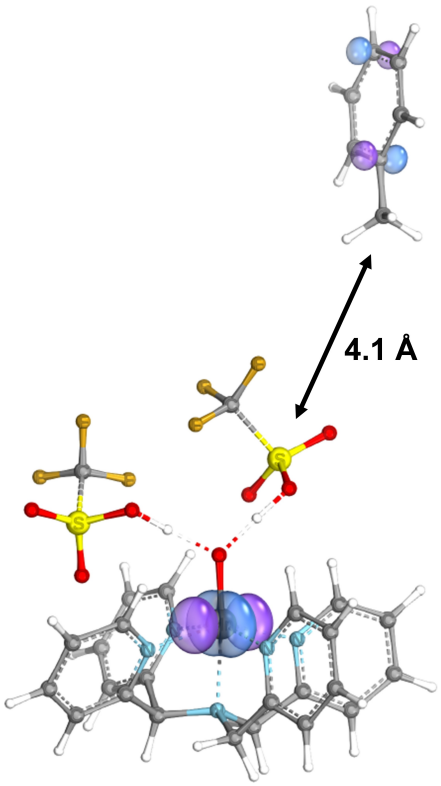

Figure 7. IBOs involved in long-range outer-sphere electron transfer between the π MO of the substrate to the $\delta(d_{xy})$ orbital of the Mn ion.

Further, the possibility of $Sc(OTf)_3$ undergoing hydrolysis in the presence of adventitious water molecule to produce a strong Bronsted acid that can facilitate the electron transfer similar to the one envisioned above cannot be ruled out.[17e] Also, we have performed calculations only for the HAT reaction with toluene as substrate, it is clear from the proposed mechanism and the experimental[9a] data that the ET mechanism is rather expected to be similar for other transformations and serves as a crucial factor in influencing the overall selectivity and reactivity of these species. It is important to note here that for oxygenation reactions such as hydroxylation, the mechanism is shown to proceed via two-steps where the second step, -OH rebound, has been shown to have substantial barriers depending on the nature of the ligand field.[17f] For the catalytic recyclability, the second step is important, and the ET mechanism here may be different to the one discussed here, and this will explored in future.

Correlations to Experiment

The computed results show that the origin for the experimentally observed singly unified electron transfer driving force[12] for both OAT and HAT reactions stems from the fact that while the substrate is at a quite longer distance from the catalyst, the HOTf molecules that are hydrogen bonded to the metal-oxo moiety transfers a proton to the metal-oxo unit while simultaneously triggering electron transfer from substrate to the metal-centre. Therefore, the ET process is primarily acid-driven, though this is found to happen only when the substrate is in the vicinity. This mechanism proposed does not require the direct involvement of substrate C–H bond activation or transfer of oxygen atoms from the metal centre to the substrate. This provides a rationale for the experimentally observed singly unified ET driving force dependence of the logarithm of the observed second-order rate constants for both OAT and HAT reactions.

Conclusions

In this study, the puzzling inner-sphere vs outer-sphere electron transfer mechanisms observed in the popular $Fe^{IV}=O$ and $Mn^{IV}=O$ species have been investigated. Our calculations demonstrate that the activation of the substrate by the catalyst is triggered first by the transfer of a proton from one of the two HOTf molecules hydrogen bonded to the metal-oxo moiety in the presence of the substrate and not by the transfer of proton/hydrogen from the substrate directly. The mechanism by which this ET takes place is primarily dictated by the type of electron (α or β) that is transferred and the type of molecular orbital ($\sigma^*(d_z^2)$ or $\delta(d_{xy})$) of the metal-oxo unit to which the electron is transferred. The mandatory spin-inversion requirement for **2-HOTf** with spin-up electron transfer to $\sigma^*(d_z^2)$ orbital of $Fe^{IV}=O$ centre and larger reorganisation energy is pinned down to be the origin for ISET mediated by one of the HOTf molecules. In the case of **1-HOTf**, a smaller reorganisation energy accompanied by choice for a spin-down electron transfer from toluene to $\delta(d_{xy})$ orbital of $Mn^{IV}=O$ unit switches the mechanism to OSET without the mediation of acid. Furthermore, the electron transfer is calculated to take place at a very long catalyst-substrate distance triggered by one of the HOTf molecules, suggesting that irrespective of the type of substrate and the reaction (epoxidation or C–H activation), it is the acid that drives the process and is the key to the reactivity. This has direct implications for the metalloenzymes, where both ET rate and reactivity are faster than biomimetic models, necessitating revised criteria for observing higher reactivity.

Computational details

The unrestricted B3LYP[19] hybrid functional has been chosen for the present study as it has already been established in the literature to be appropriate for providing a reliable electronic structure, spin-state ordering and energetics for the reactions investigated in the present study.[20] Notably, individual benchmarking studies by de Visser, Siegbahn and Li et al further affirm that the chosen methodology is reliable and appropriate for investigating the high-valent metal oxo chemistry.[21] All geometries were optimised in the gas phase, including Grimme's[22] D3 version of dispersion correction using Stuttgart/Dresden's[23] effective core potential on Mn and Fe atoms, while the 6–31G(d,p)[24] basis set was used for describing other non-metal atoms. In addition, to validate the chosen DFT methodology, the UB3LYP/SDD(6-31G**) optimised structures of **1** and **1-HOTf** were subjected to multireference (MR)[25] wave function calculation such as the complete active space self-consistent field (CASSCF) method using Douglas-Kroll-Hess (DKH) Hamiltonian contracted DKH-Def2-TZVP basis set for the metal centre and the corresponding SVP counterpart for other non-metal atoms. The CASSCF calculation was performed employing CAS(9,8) active space, which includes 3 d-electrons and 6 outer shell electrons of oxo group for Mn(IV)=O complex. The CASSCF calculations also predict the same quartet spin state as the ground state for **1-HOTf** in congruity with the DFT results, further affirming the reliability of the chosen DFT methodology (see Table S2). The optimised geometries were subjected to harmonic frequency analysis at 298.15 K to extract thermodynamic corrections and to ensure that they are global minima indeed. Further, single-point calculations were performed at a triple-zeta quality Def2TZVPP[26] basis set, including the acetonitrile solvation effect afforded by the polarisable continuum model (PCM)[27] in accordance with the experimental setup. Therefore, the energies discussed in the manuscript are zero-point energy-corrected values obtained from the UB3LYP/def2-TZVPP(MeCN) level of theory. The orbitals and electron shift diagrams were plotted from gas phase single-point calculations performed at UB3LYP/def2-TZVPP level. Since the α and β electron transfer preferences were found to be altered in the gas phases vis-à-vis solution phase single point calculations, suggesting a strong solvent-dependent mechanism at play, we have restricted the electron transfer mechanism to gas-phase energies. The ORCA 4.2.1 suite[28] was exploited to generate a Molden input file appropriate for performing intrinsic bond orbital (IBO)[29] analysis. To improve the convergence

criteria, tight self-consistent field and integration Grid5 were specified in the calculation. The spin density plots and frontier molecular orbitals were generated using Chemcraft software, while the second-order perturbation results were acquired from the natural bond orbital (NBO)[30] analysis performed at the same level of theory used for optimisation. The minimum energy crossing point (MECP) was estimated using Harvey's code.[31] All DFT calculations were performed using the Gaussian 16 suite.[32]

Acknowledgements

NJB and AS thank IITB for the postdoctoral fellowship. GR would like to thank DST and SERB (SB/SJF/2019-20/12; CRG/2022/001697) for funding.

Conflict of Interests

The authors declare no conflict of interest.

Data Availability Statement

The data that support the findings of this study are available in the supplementary material of this article.

Keywords: Nonheme metal oxo · outer sphere · inner sphere · toluene hydroxylation · electron transfer

[1] a) M. Guo, T. Corona, K. Ray, W. Nam, *ACS Cent. Sci.* **2018**, *5*, 13–28; b) K. Ray, F. F. Pfaff, B. Wang, W. Nam, *J. Am. Chem. Soc.* **2014**, *136*, 13942–13958; c) W. B. Tolman, *Activation of small molecules: organometallic and bioinorganic perspectives*, John Wiley & Sons, New Jersey, **2006**, pp. 1–357; d) A. P. Ledray, C. M. Krest, T. H. Yosca, K. Mittra, M. T. Green, *J. Am. Chem. Soc.* **2020**, *142*, 20419–20425.
[2] V. K. Yachandra, K. Sauer, M. P. Klein, *Chem. Rev.* **1996**, *96*, 2927–2950.
[3] P. R. O. De Montellano, *Cytochrome P450: structure, mechanism, and biochemistry, Vol. 3*, Springer, New York, **2005**, pp. 1–617.
[4] J. Liu, S. Chakraborty, P. Hosseinzadeh, Y. Yu, S. Tian, I. Petrik, A. Bhagi, Y. Lu, *Chem. Rev.* **2014**, *114*, 4366–4469.
[5] a) S. Fukuzumi, Y. Morimoto, H. Kotani, P. Naumov, Y.-M. Lee, W. Nam, *Nat. Chem.* **2010**, *2*, 756–759; b) H. Yoon, Y.-M. Lee, X. Wu, K.-B. Cho, R. Sarangi, W. Nam, S. Fukuzumi, *J. Am. Chem. Soc.* **2013**, *135*, 9186–9194; c) J. Park, Y. Morimoto, Y.-M. Lee, W. Nam, S. Fukuzumi, *Inorg. Chem.* **2014**, *53*, 3618–3628; d) J. Park, Y.-M. Lee, W. Nam, S. Fukuzumi, *J. Am. Chem. Soc.* **2013**, *135*, 5052–5061; e) P. Comba, H. Fukuzumi S Fau - Kotani, S. Kotani H Fau - Wunderlich, S. Wunderlich; f) K. Warm, I. Monte Pérez, U. Kuhlmann, P. Hildebrandt, E. Farquhar, M. Swart, K. Ray, *Z. Anorg. Allg. Chem.* **2021**, *647*, 1495–1502; g) D. G. Karmalkar, M. S. Seo, Y.-M. Lee, Y. Kim, E. Lee, R. Sarangi, S. Fukuzumi, W. Nam, *Inorg. Chem.* **2021**, *60*, 16996–17007; h) D. Sun, Z. Wu, X. Zhang, J. Yang, Y. Zhao, W. Nam, Y. Wang, *J. Am. Chem. Soc.* **2023**, *145*, 5739–5749; i) J. Park, Y. Morimoto, Y.-M. Lee, W. Nam, S. Fukuzumi, *J. Am. Chem. Soc.* **2012**, *134*, 3903–3911.
[6] R. A. Marcus, *Angew. Chem. Int. Ed. Engl.* **1993**, *32*, 1111–1121.
[7] M.-H. Baik, B. F. Gherman, R. A. Friesner, S. J. Lippard, *J. Am. Chem. Soc.* **2002**, *124*, 14608–14615.
[8] H. Bataineh, O. Pestovsky, A. Bakac, *Inorg. Chem.* **2016**, *55*, 6719–6724.
[9] a) N. Sharma, Y.-M. Lee, X.-X. Li, W. Nam, S. Fukuzumi, *Inorg. Chem.* **2019**, *58*, 13761–13765; b) A. A. Massie, M. C. Denler, R. Singh, A. Sinha, E. Nordlander, T. A. Jackson, *Chem. Eur. J.* **2020**, *26*, 900–912.
[10] S. Fukuzumi, *Coord. Chem. Rev.* **2013**, *257*, 1564–1575.
[11] A. Sen, R. Kumar, G. Rajaraman, *Inorg. Chim. Acta* **2022**, *529*, 120654.
[12] M. Puri, L. Que Jr, *Acc. Chem. Res.* **2015**, *48*, 2443–2452.
[13] J. Chen, H. Yoon, Y.-M. Lee, M. S. Seo, R. Sarangi, S. Fukuzumi, W. Nam, *Chem. Sci.* **2015**, *6*, 3624–3632.
[14] D. Janardanan, Y. Wang, P. Schyman, L. Que Jr, S. Shaik, *Angew. Chem.* **2010**, *122*, 3414–3417.
[15] a) Y.-M. Lee, H. Kotani, T. Suenobu, W. Nam, S. Fukuzumi, *J. Am. Chem. Soc.* **2008**, *130*, 434–435; b) J. Park, Y. Morimoto, Y.-M. Lee, W. Nam, S. Fukuzumi, *J. Am. Chem. Soc.* **2012**, *134*, 3903–3911.
[16] J. N. Harvey, M. Aschi, H. Schwarz, W. Koch, *Theor. Chem. Acc.* **1998**, *99*, 95–99.
[17] a) S. Shaik, H. Chen, D. Janardanan, *Nat. Chem.* **2011**, *3*, 19–27; b) A. Sen, R. Kumar, G. Rajaraman, *Handbook of CH-Functionalization*, John Wiley & Sons, Ltd, New Jersey, **2022**, pp. 1–47; c) I. M. Perez, X. Engelmann, Y.-M. Lee, M. Yoo, E. Kumaran, E. R. Farquhar, E. Bill, J. England, W. Nam, M. Swart, K. Ray, *Angew. Chem. Int. Ed.* **2017**, *56*, 14384–14388.; d) S. Munshi, A. Sinha, S. Yiga, S. Banerjee, R. Singh, M. K. Hossain, M. Haukka, A. F. Valiati, R. D. Huelsmann, E. Martendal, R. Peralta, F. Xavier, O. F. Wendt, T. K. Paine, E. Nordlander, *Dalton Trans.* **2022**, *51*, 870–884; e) J. D. Steen, S. Stepanovic, M. Parvizian, J. W. d. Boer, R. Hage, J. Chen, M. Swart, M. Gruden, W. R. Browne, *Inorg. Chem.* **2019**, *58*, 14924–14930; f) R. Kumar, A. Ansari, P. Comba, G. Rajaraman, *Chem. Eur. J.* **2023**, Submitted.
[18] a) R. A. Marcus, *J. Chem. Phys.* **2004**, *24*, 966–978; b) R. A. Marcus, N. Sutin, *Biochim. Biophys. Acta Bioenerg.* **1985**, *811*, 265–322.
[19] a) A. D. Becke, *Phys. Rev. A* **1988**, *38*, 3098–3100; b) A. D. Becke, *J. Chem. Phys.* **1993**, *98*, 5648–5652; c) A. D. Becke, *J. Chem. Phys.* **1997**, *107*, 8554–8560.
[20] a) M. Jaccob, A. Ansari, B. Pandey, G. Rajaraman, *Dalton Trans.* **2013**, *42*, 16518–16526; b) A. Ansari, A. Kaushik, G. Rajaraman, *J. Am. Chem. Soc.* **2013**, *135*, 4235–4249; c) A. Sen, N. Vyas, B. Pandey, M. Jaccob, G. Rajaraman, *Isr. J. Chem.* **2020**, *60*, 973–986.
[21] a) X. Sun, C. Geng, R. Huo, U. Ryde, Y. Bu, J. Li, *J. Phys. Chem.* **2014**, *118*, 1493–1500; b) P. E. M. Siegbahn, T. Borowski, *Acc. Chem. Res.* **2006**, *39*, 729–738; c) M. G. Quesne, D. Senthilnathan, D. Singh, D. Kumar, P. Maldivi, A. B. Sorokin, S. P. de Visser, *ACS Catal.* **2016**, *6*, 2230–2243.
[22] a) S. Grimme, S. Ehrlich, L. Goerigk, *J. Comput. Chem.* **2011**, *32*, 1456–1465; b) S. Grimme, J. Antony, S. Ehrlich, H. Krieg, *J. Chem. Phys.* **2010**, *132*, 154104.
[23] P. Fuentealba, H. Preuss, H. Stoll, L. Von Szentpály, *Chem. Phys. Lett.* **1982**, *89*, 418–422.
[24] W. J. Hehre, R. Ditchfield, J. A. Pople, *J. Chem. Phys.* **2003**, *56*, 2257–2261.
[25] C. A. Gaggioli, S. J. Stoneburner, C. J. Cramer, L. Gagliardi, *ACS Catal.* **2019**, *9*, 8481–8502.
[26] a) F. Weigend, *Phys. Chem. Chem. Phys.* **2006**, *8*, 1057–1065; b) F. Weigend, R. Ahlrichs, *Phys. Chem. Chem. Phys.* **2005**, *7*, 3297–3305.
[27] J. Tomasi, B. Mennucci, R. Cammi, *Chem. Rev.* **2005**, *105*, 2999–3094.
[28] F. Neese, *WIREs Comput. Mol. Sci.* **2012**, *2*, 73–78.
[29] G. Knizia, J. E. M. N. Klein, *Angew. Chem. Int. Ed.* **2015**, *54*, 5518–5522.
[30] F. Martin, H. Zipse, *J. Comput. Chem.* **2005**, *26*, 97–105.
[31] a) J. N. Harvey, *WIREs Comput. Mol. Sci.* **2014**, *4*, 1–14; b) T. Yang, M. G. Quesne, H. M. Neu, F. G. Cantú Reinhard, D. P. Goldberg, S. P. de Visser, *J. Am. Chem. Soc.* **2016**, *138*, 12375–12386.
[32] M. Frisch, G. Trucks, H. Schlegel, G. Scuseria, M. Robb, J. Cheeseman, G. Scalmani, V. Barone, G. Petersson, H. Nakatsuji, *Wallingford CT* **2016**, *421*.
[33] J. Zhang, Y.-M. Lee, M. S. Seo, Y. Kim, E. Lee, S. Fukuzumi, W. Nam, *Inorg. Chem. Front.* **2022**, *9*, 3233–3243.
[34] N. Sharma, H.-B. Zou, Y.-M. Lee, S. Fukuzumi, W. Nam, *J. Am. Chem. Soc.* **2021**, *143*, 1521–1528.
[35] Y.-M. Lee, S. Kim, K. Ohkubo, K.-H. Kim, W. Nam, S. Fukuzumi, *J. Am. Chem. Soc.* **2019**, *141*, 2614–2622.

Manuscript received: September 5, 2023
Revised manuscript received: October 12, 2023
Accepted manuscript online: October 19, 2023
Version of record online: November 6, 2023